One- and Two-Photon Excited Fluorescence Lifetimes and Anisotropy Decays of Green Fluorescent Proteins

ARTICLE *in* BIOPHYSICAL JOURNAL · APRIL 2000

Impact Factor: 3.97 · DOI: 10.1016/S0006-3495(00)76711-7 · Source: PubMed

4 AUTHORS, INCLUDING:

Vinod Subramaniam
VU University Amsterdam
270 PUBLICATIONS **5,952** CITATIONS

One- and Two-Photon Excited Fluorescence Lifetimes and Anisotropy Decays of Green Fluorescent Proteins

Andreas Volkmer,* Vinod Subramaniam,† David J. S. Birch,* and Thomas M. Jovin†

*Photophysics Research Group, Department of Physics and Applied Physics, University of Strathclyde, 107 Rottenrow, Glasgow G4 ONG, Scotland, United Kingdom; and †Department of Molecular Biology, Max Planck Institute for Biophysical Chemistry, Am Fassberg 11, D-37077 Göttingen, Germany

ABSTRACT We have used one- (OPE) and two-photon (TPE) excitation with time-correlated single-photon counting techniques to determine time-resolved fluorescence intensity and anisotropy decays of the wild-type Green Fluorescent Protein (GFP) and two red-shifted mutants, S65T-GFP and RSGFP. WT-GFP and S65T-GFP exhibited a predominant ~3 ns monoexponential fluorescence decay, whereas for RSGFP the main lifetimes were ~1.1 ns (main component) and ~3.3 ns. The anisotropy decay of WT-GFP and S65T-GFP was also monoexponential (global rotational correlation time of 16 ± 1 ns). The ~1.1 ns lifetime of RSGFP was associated with a faster rotational depolarization, evaluated as an additional ~13 ns component. This feature we attribute tentatively to a greater rotational freedom of the anionic chromophore. With OPE, the initial anisotropy was close to the theoretical limit of 0.4; with TPE it was higher, approaching the TPE theoretical limit of 0.57 for the colinear case. The measured power dependence of the fluorescence signals provided direct evidence for TPE. The general independence of fluorescence decay times, rotation correlation times, and steady-state emission spectra on the excitation mode indicates that the fluorescence originated from the same distinct excited singlet states (A*, I*, B*). However, we observed a relative enhancement of blue fluorescence peaked at ~440 nm for TPE compared to OPE, indicating different relative excitation efficiencies. We infer that the two lifetimes of RSGFP represent the deactivation of two substates of the deprotonated intermediate (I*), distinguished by their origin (i.e., from A* or B*) and by nonradiative decay rates reflecting different internal environments of the excited-state chromophore.

INTRODUCTION

Two-photon excitation (TPE) has developed as an important alternative to traditional one-photon excitation (OPE) in fluorescence microscopy and spectroscopy (Denk et al., 1990; Bennett et al., 1996; Malak et al., 1997; Svoboda et al., 1997; Bewersdorf et al., 1998). The intrinsic advantages of the two-photon process include reduced background fluorescence from fluorophores outside the focal volume, decreased photobleaching, inherent optical sectioning capability, and lower photodamage of sensitive biological samples (Denk et al., 1995). TPE is also directly applicable to a new class of fluorophore that is revolutionizing the visualization of biological systems and molecular interactions, the Green Fluorescent Protein (GFP) from the jellyfish *Aequoria victoria*, and its mutants (Xu et al., 1996; Tsien, 1998).

The various GFPs have attracted enormous attention in recent years as important reporters in cell, developmental, and molecular biology (for a comprehensive overview see Tsien (1998) and references therein). When fused to proteins of interest and expressed in vivo, GFP acts as a versatile indicator of structure and function within cells (Misteli and Spector, 1997) and can be visualized using standard microscopy techniques (Niswender et al., 1995; Presley et al., 1997) and multiphoton excitation (MPE) microscopy (Kohler et al., 1997). GFP and its constructs are being increasingly used in fluorescence lifetime imaging microscopy (FLIM) and fluorescence resonance energy transfer (FRET) modes of microspectroscopy for the visualization of protein-protein interactions, signaling, and trafficking in cellular systems (Bastiaens and Jovin, 1996; Miyawaki et al., 1997; Mahajan et al., 1998; Ng et al., 1999). The measurement of excited-state fluorescence lifetimes allows the discrimination of fluorophores with similar spectral emission properties. It is therefore of primary importance to understand the fundamental photophysical characteristics of GFP and its mutants at the typical excitation wavelengths used in two-photon microscopy systems (e.g., 800 nm excitation from titanium:sapphire lasers). Early work by Ward (Perozzo et al., 1988) and Prendergast (Nageswara Rao et al., 1980) established the fluorescence lifetime and anisotropy of GFP, and recent experiments have characterized in greater detail the OPE photophysical properties of some GFPs (Chattoraj et al., 1996; Lossau et al., 1996; Patterson et al., 1997; Kummer et al., 1998; Striker et al., 1999), including an extensive study of pH-dependent photophysics (Haupts et al., 1998). However, there have been no detailed comparisons of the OPE and TPE fluorescence properties of GFPs in the literature.

In this report we focus on the time-resolved detection of the TPE fluorescence intensity and anisotropy decays, and compare OPE and TPE at 400 nm and 800 nm, respectively, of the wild-type GFP and two mutant forms of the protein, the S65T mutant (in which Ser-65 is replaced by Thr) and a

Received for publication 21 June 1999 and in final form 3 December 1999.

Address reprint requests to Dr. Thomas M. Jovin, Dept. of Molecular Biology, Max Planck Institute for Biophysical Chemistry, Am Fassberg 11, D-37077 Göttingen, Germany. Tel.: 49-551-2011382; Fax: 49-551-2011467; E-mail: tjovin@mpc186.mpibpc.gwdg.de.

Andreas Volkmer's present address is Dept. of Chemistry and Chemical Biology, Harvard University, 12 Oxford St., Cambridge, MA 02138.

0006-3495/00/03/1589/10 $2.00

mutant exhibiting a red-shifted absorption peak (RSGFP; bearing the substitutions F64M, S65G, Q69L). The different selection rules for one-photon and two-photon excitation provide insight into the properties of excited states not accessible by one-photon spectroscopy. Furthermore, time-resolved multiphoton techniques permit the monitoring of the rotational diffusion and population decay of the excited molecule under unusual conditions, and thus constitute a new tool for structural and dynamic studies.

THEORETICAL BACKGROUND

TPE of a fluorophore involves the absorption of two photons in the same quantum event generating an electronically excited state, followed by the subsequent spontaneous emission of another (generally higher-energy) photon at the characteristic wavelength of fluorophore emission. This induced fluorescence signal displays a squared dependence on the exciting optical power. The basic equation relating the number of fluorescence photons emitted per molecule and unit time $I^{(2)}(t)$ (in the absence of saturation, self-quenching, photobleaching, or stimulated emission) to the experimental parameters for TPE is given by Xu and Webb (1996)

$$I^{(2)}(t) \propto \frac{\Phi}{2}\sigma_2\rho^2 \tag{1}$$

where Φ is the fluorescence quantum yield of the molecule, σ_2 the two-photon absorption cross-section, and ρ the incident photon flux density. The factor 2 in the denominator reflects the fact that two photons are required for each absorption event. Since TPE is essentially an instantaneous process, the peak incident photon flux density of a pulsed laser source ρ_{peak} determines the excitation rate.

Excitation of a randomly oriented molecular system with plane-polarized light creates an anisotropic orientational distribution of excited molecules that is markedly more different with TPE than with OPE. A complex analysis is necessary for a complete description of two-photon phenomena (Callis, 1993; Chen and VanDerMeer, 1993; Wan and Johnson, 1994). In the special case of a fluorescent probe with cylindrical symmetry and one dominating two-photon transition tensor element excited with plane-polarized identical photons, the initial anisotropy upon TPE, $r_0^{(2)}$, (before any rotational diffusion) can be expressed by the general equation that also accommodates the OPE case:

$$r_0^{(l)} = \frac{2l}{2l+3}\left[\frac{3}{2}\cos^2\beta - \frac{1}{2}\right] \tag{2}$$

where l is the number of photons involved in the excitation process and β is the angle between the dominant absorption and emission transition moment (Gryczynski et al., 1995). For the colinear case ($\beta = 0$) it is expected that increasing the number of photons leads to a more highly oriented excited-state population. Thus, the maximal anisotropies for OPE and TPE are 2/5 and 4/7, respectively, highlighting the potentially higher dynamic range of TPE in time-resolved anisotropy measurements. Values of $r_0^{(1)}$ reported by Partikian et al. (1998) and in this work approach the limiting value of 0.4, supporting the assumption that $\beta \approx 0$ for GFPs.

For this special TPE case (emission transition moment colinear with dominating two-photon transition tensor element) the total time-dependent fluorescence intensity can be measured under the same conditions as for OPE to suppress the effects of molecular rotation. The emission is monitored through a polarizer placed at 54.7° relative to the polarization direction of excitation (Lakowicz et al., 1992; Wan and Johnson, 1994). The fluorescence decay curves, $F^{(l)}(t)$, are presumed to obey a multiexponential decay law

$$F^{(l)}(t) = \alpha_0 + \sum_{k=1}^{n} \alpha_k e^{-t/\tau_k} \tag{3}$$

where τ_k is the kth fluorescence (lifetime) decay component with a corresponding amplitude α_k, and α_0 is a constant background (generally negligible). The fractional steady-state intensity associated with component k is given by

$$f_k = \alpha_k\tau_k \Big/ \sum_{i=1}^{n} \alpha_i\tau_i \tag{4}$$

The time-dependent emission anisotropy is determined for fluorescence decay curves recorded with the analyzing polarizer oriented parallel, $F_{\parallel}^{(l)}(t)$, and perpendicular, $F_{\perp}^{(l)}(t)$, to the linearly polarized excitation light. The total anisotropy decay of a mixture of fluorophores is analyzed according to:

$$r^{(l)}(t) = \frac{F_{\parallel}^{(l)}(t) - F_{\perp}^{(l)}(t)}{F_{\parallel}^{(l)}(t) + 2F_{\perp}^{(l)}(t)} = \frac{\sum_{k=1}^{n} \alpha_k e^{-t/\tau_k} r_{0k}^{(l)}\, e^{-t/\phi_k}}{\sum_{k=1}^{n} \alpha_k e^{-t/\tau_k}} \tag{5}$$

where α_0 has been omitted for clarity. The right-hand term of Eq. 5 corresponds to a kinetic model for n fluorescent species characterized by an excited-state lifetime, τ_k, rotational correlation time, ϕ_k, and initial anisotropy $r_{0k}^{(l)}$ (Jovin et al., 1982). The individual rotational correlation times represent the combined global and local depolarizing motions of the particular domain of the macromolecule associated with the particular deactivation pathway. We assume that all species share the global rotational correlation time of the macromolecule such that the ϕ_k can be factored in the form

$$\phi_k^{-1} \simeq \phi_{global}^{-1} + \phi_{local,k}^{-1} \tag{6}$$

The fact that the rotational correlation times for GFP are much longer than the excited-state lifetimes does not justify a more sophisticated decomposition into eigenvector components.

MATERIALS AND METHODS

GFPs

Wild-type (WT), and mutants [S65T, bearing a single amino acid substitution; RSGFP, with the three substitutions F64M, S65G, Q69L (Delagrave et al., 1995)] of the cloned *A. victoria* GFP in the expression vector pRSETa (Invitrogen, Carlsbad, CA) were used. These plasmids, a gift of Dr. Rolando Rivera-Pomar (MPIbpc, Göttingen, Germany), code for expression of the GFP open reading frame with an additional six histidines at the amino terminus, under control of the T7 promoter inducible by isopropyl-β-D-thiogalactoside. The histidine tag permits purification of the recombinant protein using standard procedures with a Ni-chelating resin (Ni-NTA-Agarose, Qiagen, Hilden, Germany). Protein purity was confirmed by SDS-PAGE. Further purification was performed as required with Pharmacia Superdex-75 size-exclusion chromatography. The purified protein was dialyzed extensively against 10 mM sodium phosphate buffer, pH 7.0, concentrated, and stored. All spectroscopic measurements were carried out with ~18 μM protein dissolved in 10 mM Tris-HCl buffer, pH 8.0, 0.1 M NaCl at room temperature (~22°C).

Fluorescence spectroscopy

Details of the experimental configuration consisting of a femtosecond titanium:sapphire laser system, a time-correlated single-photon counting (TCSPC) arrangement for time-resolved detection, and an optical fiber-coupled CCD spectrophotometer (Oriel MS127i/INSTASPEC) for steady-state spectral measurements were described previously (Volkmer et al., 1997). Briefly, a regeneratively amplified titanium:sapphire mode-locked laser system (800 nm excitation, 250 kHz repetition rate, 180 fs pulsewidth; Coherent Mira 900/RegA 9000) was used to generate pulses of up to 4 μJ energy. OPE at the same effective energy as 800 nm TPE was achieved by frequency doubling the titanium:sapphire fundamental output.

For fluorescence decay measurements a Glan Taylor prism polarizer was oriented at the magic angle (54.7°) relative to the polarization vector of the excitation beam to suppress the contributions of rotational depolarization to the fluorescence decay signal (see Theory section). Fluorescence anisotropy decay measurements were carried out by recording the fluorescence with the polarizer alternating between parallel and perpendicular orientations to the excitation polarization, with a dwell time of 30 s in each position to correct for excitation intensity drifts. The emerging light was imaged onto a microchannel plate photomultiplier detector (MCP-PM; Hamamatsu R1712U-03). Fluorescence decays were collected using standard TCSPC electronics in 1K channels at 0.0675 ns/ch.

In the time-resolved measurements the emission was spectrally isolated using bandpass interference filters with center wavelengths at 456 nm (FWHM = 70 nm) and 514 nm (FWHM = 8 nm). Additional steady-state fluorescence measurements were performed on an SLM 8000C fluorimeter and used to determine the relative quantum yields.

Data analysis

Least-squares re-convolution fits of fluorescence intensity decay records were carried out using the IBH decay analysis software library (IBH Consultants Ltd., Glasgow, Scotland). Inasmuch as the instrumental response function of this setup was ~50 ps FWHM (compared to nanosecond decay times), the experimental anisotropy decay curves were fitted to the above model to give an estimate of the anisotropy decay parameter without a deconvolution correction for the finite instrumental response time. Errors are reported as ±3 standard deviations, as determined by the fits to the data. We note the inherently large inaccuracy in determining rotational correlation times that are an order of magnitude larger than the corresponding fluorescence lifetime. Errors for the RSGFP anisotropy decays were derived from least-square fit results using Kaleidagraph (Synergy Software, Reading, PA).

RESULTS

Steady-state spectra

WT-GFP and the S65T and RSGFP mutants excited at 800 nm yielded the fluorescence spectra displayed in Fig. 1. The characteristic GFP bands had peaks at ~511 nm in the case of WT-GFP and RSGFP, and ~514 nm for S65T-GFP, and were almost indistinguishable from those observed with OPE at 400 nm. However, small differences emerged upon more detailed analysis of the wavelength region around 550 nm and the weak emission band at ~440 nm. The relative intensities of both spectral features increased upon excitation at 800 nm compared to 400 nm excitation. For OPE at 400 nm, the relative fluorescence intensity of the 440 nm band of S65T-GFP was approximately twice that of WT-GFP or RSGFP. For TPE with 800 nm photons, however, the relative intensities of the blue emission bands of both S65T- and WT-GFP were similar, whereas RSGFP showed comparatively low levels of 440 nm fluorescence.

For excitation at both 400 nm (λ_{exc} used in the time-resolved fluorescence experiments) and 490 nm (peak of the absorption), the emission quantum yield (Φ) of RSGFP was estimated to be 0.30 times that of S65T-GFP by comparing

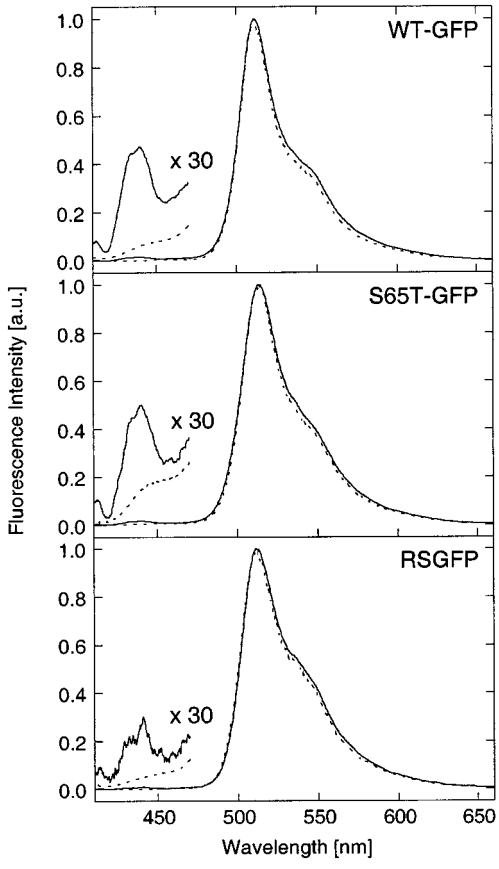

FIGURE 1 Normalized steady-state OPE (λ_{exc} = 400 nm; *dashed lines*) and TPE (λ_{exc} = 800 nm; *solid lines*) fluorescence emission spectra of WT-GFP, S65T-GFP, and RSGFP.

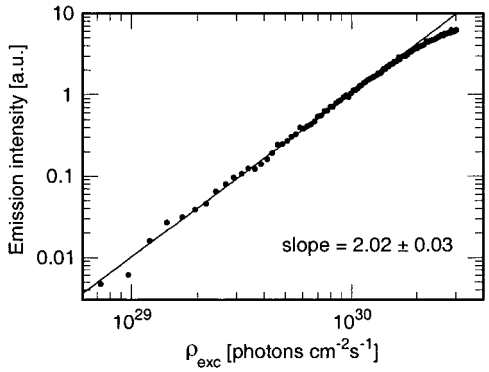

FIGURE 2 Log-log plot of the fluorescence emission (514 nm) of RS-GFP versus the incident photon flux density for TPE excitation at 800 nm. A linear regression fit for photon flux densities $\leq 1.6 \times 10^{30}$ photons cm^{-2} s^{-1} yields a slope of 2.02 ± 0.03, confirming the two-photon nature of the excitation. Saturation of the fluorescence is observed for higher photon flux densities.

the integrated emission from samples of S65T-GFP and RSGFP normalized by the absorbance at the excitation wavelength. For RSGFP, this yields an absolute value of $\Phi \sim 0.19$ based upon the published value of 0.64 for S65T-GFP (Patterson et al., 1997).

Excitation power dependence

The power dependence of the fluorescence detected at 514 nm was determined from a log-log plot of the fluorescence signal versus incident peak photon flux density (shown in Fig. 2 for RSGFP). For photon flux densities $\leq 1.6 \times 10^{30}$ photons cm^{-2} s^{-1}, the induced fluorescence obeyed a power-squared intensity dependence as indicated by the measured slope of 2.02 ± 0.03, thereby confirming the existence of TPE. However, a decrease in the apparent power exponent was observed for larger irradiances. All time-resolved measurements were carried out at the lower intensity levels at which deviations from the second-order power law were absent.

Fluorescence intensity decays

The analyses of the time-resolved fluorescence intensity decay measurements performed under magic angle conditions are summarized in Table 1. The measured fluorescence decays of WT- and S65T-GFP were predominantly monoexponential with a fluorescence lifetime of ~3 ns. With both OPE and TPE the emission at 514 nm was well-described by this single decay time, whereas better fits to the 456 nm emission data were obtained with a biexponential decay model yielding a small additional subnanosecond component of ~0.2 ns. While WT-GFP and S65T-GFP showed almost identical fluorescence decay kinetics, i.e., monoexponential at 514 nm and biexponential at 456 nm emission, RSGFP did not follow the same trend. The fluorescence decay curves of RSGFP were best described by a three-exponential decay model with lifetimes of ~0.4, ~1.1, and ~3.3 ns, and similar fractional intensities at both observation wavelengths.

Based on the quantum yields for S65T-GFP and RSGFP (see above), and fluorescence lifetimes measured at 514 nm for S65T-GFP and RSGFP (Table 1), and the radiative scheme of Fig. 4 we calculated the radiative (k_f) and non-radiative (k_{NR}) decay rates for both proteins according to the relations $\Phi = k_f \Sigma \alpha_i \tau_i$, where $\tau_i = (k_f + k_{NR,i})^{-1}$. For S65T-GFP we used the single lifetime $\tau = 3.01$ ns, while for RSGFP we used the two longer lifetime components ($i = 2, 3$; see Table 1), since the subnanosecond component associated with deactivation of the protonated species A* is not monitored at this emission wavelength and, hence, its contribution to the total quantum yield is negligible. These parameters yield $k_f^{S65T} \approx 2.1 \times 10^8$ s^{-1}, $k_{NR}^{S65T} \approx 1.2 \times 10^8$ s^{-1}, and $k_f^{RSGFP} \approx 1.4 \times 10^8$ s^{-1}. Assuming that the calculated k_f is unique for RSGFP (since it is associated

TABLE 1 Analysis of one- and two-photon-induced fluorescence intensity decays of WT-GFP, S65T-GFP, and RSGFP; see text for definitions

GFP	λ_{em} (nm)	λ_{exc} = 400 nm (OPE)				λ_{exc} = 800 nm (TPE)			
		τ_k (ns)	α_k	f_k	χ^2	τ_k (ns)	α_k	f_k	χ^2
WT-GFP	514	3.16 ± 0.03	1.00	1.00	1.08	3.10 ± 0.03	1.00	1.00	1.05
	456	0.20 ± 0.07	0.50	0.06	1.01	0.17 ± 0.06	0.43	0.04	1.03
		3.11 ± 0.04	0.50	0.94		3.03 ± 0.04	0.57	0.96	
S65T-GFP	514	3.01 ± 0.02	1.00	1.00	0.99	2.96 ± 0.03	1.00	1.00	1.08
	456	0.23 ± 0.02	0.67	0.14	1.05	0.17 ± 0.02	0.47	0.05	1.10
		2.91 ± 0.05	0.33	0.86		2.82 ± 0.03	0.53	0.95	
RSGFP	514	0.47 ± 0.20	0.13	0.05	1.09	0.35 ± 0.16	0.11	0.03	1.25
		1.13 ± 0.03	0.78	0.70		1.10 ± 0.02	0.83	0.79	
		3.41 ± 0.27	0.09	0.25		3.24 ± 0.30	0.06	0.18	
	456	0.33 ± 0.11	0.15	0.04	1.15	0.34 ± 0.15	0.13	0.04	1.16
		1.09 ± 0.03	0.73	0.64		1.11 ± 0.02	0.78	0.72	
		3.32 ± 0.25	0.12	0.32		3.30 ± 0.25	0.09	0.24	

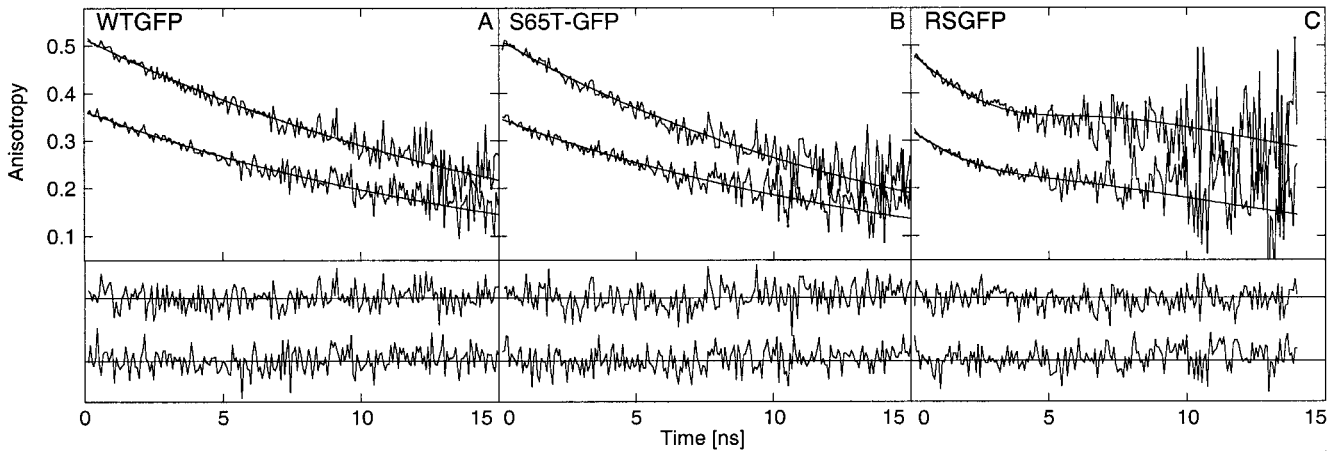

FIGURE 3 Time-resolved fluorescence anisotropy decays of WT-GFP (*A*), S65T-GFP (*B*), and RSGFP (*C*) upon OPE at 400 nm (*lower curve* in each panel) and TPE at 800 nm. Fits to a monoexponential anisotropy decay model are shown for *A* and *B*. The decay model for RSGFP is discussed in the text. Residuals for all fits are indicated (OPE: *lower curve*).

with the chromophore in the I* configuration; see Fig. 4), we estimate that the nonradiative decay rates associated with the 1.1 ns and 3.3 ns lifetimes are $k_{NR}^{RSGFP,1.1ns} \approx 7.4 \times 10^8\ s^{-1}$ and $k_{NR}^{RSGFP,3.3ns} \approx 1.5 \times 10^8\ s^{-1}$, respectively.

Fluorescence anisotropy decays

Fluorescence anisotropy decays were monitored at 514 nm for all three types of GFP and are shown in Figure 3. The anisotropy parameters obtained from fitting the experimental data to Eq. 5 are summarized in Table 2.

As in the case of the fluorescence intensity decay measurements, WT- and S65T-GFP exhibited almost identical fluorescence anisotropy kinetics (Fig. 3, *A* and *B*). The initial anisotropy for 400 nm excitation was ~0.35. TPE at 800 nm, however, resulted in an r_0 of ~0.51, exceeding the one-photon value. The measured fluorescence anisotropy decays of WT-GFP and S65T-GFP were best described by an isotropic rotational motion of the chromophore with a monoexponential decay characterized by a rotational correlation time of ~16 ns.

TABLE 2 Analysis of one- and two-photon-induced fluorescence anisotropy decays of WT-GFP, S65T-GFP, and RS-GFP monitored at 514 nm emission wavelength assuming a global rotational correlation constant

GFP	λ_{exc} (nm)	ϕ_{global} (ns)	$\phi_{local,2}$ (ns)	$r_0^{(l)}$	χ^2
WT-GFP	400	16 ± 1		0.36	1.01
	800	17 ± 1		0.51	0.95
S65T-GFP	400	16 ± 1		0.34	0.90
	800	15 ± 1		0.51	1.16
RSGFP	400	17 ± 1	13 ± 1	0.32	1.17
	800	27 ± 3	13 ± 1	0.48	0.92

The correlation time corresponding to the second lifetime ($k = 2$ in Eq. 5) was analyzed according to Eq. 6.

In comparison to WT- and S65T-GFP, RSGFP exhibited markedly different fluorescence anisotropy decay at 514 nm. It was not possible to fit the OPE and TPE anisotropy decay curves with a monoexponential model. Two versions of Eq. 5 were explored further. In one, a unique correlation time ϕ_{global} was assumed, but the initial anisotropies ($r_{0k}^{(l)}$) of the three decay components were allowed to vary. No parameter set was found that could adequately represent the anisotropy curve in this manner. In the second approach, the $\tau_2 = 1.1$ ns decay component unique to RSGFP was assigned an additional rotational correlation term $\phi_{local,2}$ (Eq. 6). The total decay function (denominator of Eq. 5) was fitted using the lifetimes from Table 1 and the resulting decay parameters (Eq. 3) were used to fit the difference curve (numerator of Eq. 5). The results were very satisfactory, yielding (for OPE) a ϕ_{global} of ~17 ns, a global r_0 value of 0.32, and an additional rotational correlation term ($\phi_{local,2} \approx 13$ ns) corresponding to the 1.1 ns lifetime. The same procedure, applied to the TPE data, yielded a higher ϕ_{global} of ~27 ns, a global r_0 value of 0.48, and $\phi_{local,2} \approx$ 13 ns. Note that the determination of rotational correlation times that are significantly longer than the corresponding fluorescence lifetimes is inherently difficult and prone to errors. Fixing ϕ_{global} to a value <20 ns did not lead to an appreciable reduction in the quality of the fit. The resulting anisotropy functions (OPE/TPE) are shown in Fig. 3 *C*. For all three proteins, measurements with a fivefold increased time resolution did not yield evidence for a fast anisotropy decay in the subnanosecond range.

DISCUSSION

Decay scheme for GFPs

To interpret the data for RSGFP in terms of a model applicable for S65T- and WT-GFP, we invoke a modified

excited-state proton transfer (ESPT) reaction scheme (Fig. 4). ESPT has been proposed on structural grounds (Brejc et al., 1997; Palm et al., 1997) and used to interpret the photophysical characteristics of GFP and its mutants in the frequency and time domain excited via OPE (Chattoraj et al., 1996; Lossau et al., 1996).

The model is comprised of a protonated state of GFP (absorption peak at ~400 nm, termed A), a deprotonated state (absorption peak at ~480–490 nm, B), and an intermediate deprotonated species I. Recent high-resolution spectral hole-burning experiments on wild-type GFP at cryotemperatures have directly identified the intermediate I in the ground state and established the 0-0 transition of all three species (Creemers et al., 1999). OPE at 400 nm and TPE at 800 nm result in the excitation of the protonated (A) and deprotonated (B) ground states of the chromophore. In WT-GFP at pH 8 the A ground-state absorption is dominant, whereas in S65T-GFP and RSGFP the equilibrium in the ground state is strongly shifted toward the deprotonated molecular forms.

Depopulation of A* occurs via 1) highly dispersive ESPT on the picosecond time scale (Chattoraj et al., 1996; Lossau et al., 1996) forming an excited deprotonated species in the A configuration (I*) [which cannot achieve an equilibrium conformation during its short lifetime (Lossau et al., 1996)]; 2) photoconversion between A* and B [photochromicity, (Striker et al., 1999)]; and 3) radiative and nonradiative deactivation processes to the ground state. The radiative transition manifests itself as a weak blue emission at ~440 nm, indicating that the dominant depopulation channel of A* is via ESPT to I*.

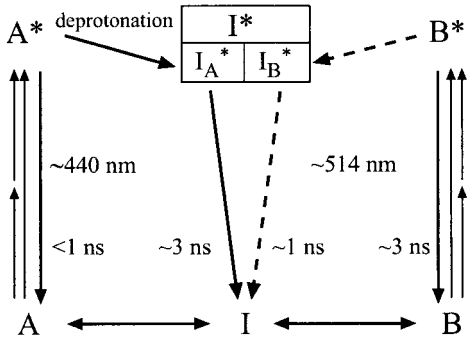

FIGURE 4 Decay scheme for GFPs, adapted from excited state proton transfer models (Chattoraj et al., 1996; Lossau et al., 1996). A, protonated species; B, deprotonated species; I, deprotonated intermediate species. The corresponding excited states (upon OPE at 400 nm or TPE at 800 nm) are denoted by asterisks. As found in this work, A* and B* transfer to I*; the chromophore environment in I* is assumed to reflect the excitation history of the state, and thus two substates are invoked, I_A^* and I_B^*, with different characteristic nonradiative decay rates. The B* → I* transition is not accessible in WT-GFP and S65T, but is favored in RSGFP, (*dashed arrows*; Creemers et al., 1999; Creemers et al., 2000). Interconversion between I_A^* and I_B^* is presumed to be negligible during the excited state lifetime. Approximate lifetimes and emission peaks are assigned to each decay path. In the case of WT- and S65T-GFP the green emission arises from both I* and B*. High-resolution experiments on WT-GFP have resolved the lifetimes associated with these states as ~3.3 ns and ~2.8 ns, respectively (Striker et al., 1999) (see text for discussion).

The green emission is thought to originate from both the I* and B* forms. The competing B* → I* transition following excitation into the B* state is dependent on the height of the corresponding energetic barrier. The energy schemes of various GFPs have been estimated by high-resolution hole-burning and excitation/emission spectroscopy (Creemers et al., 1999; Creemers et al., 2000); they depend strongly on the specific amino acid substitutions. Thus, the B* → I* transition does not occur in WT-GFP (Creemers et al., 1999) or S65T, but is energetically favored in RSGFP (Creemers et al., 2000; also see below). In the scheme of Fig. 4 we postulate that the excited electronic intermediate state I* may be distinguished by an excitation-history-dependent intramolecular (chromophore) environment; that is, whether I* is accessed via the A* or the B* manifolds. The terminology I_A^* and I_B^* denotes these substates, each of which is presumed to have a (different) characteristic nonradiative decay rate reflecting the subtle differences in chromophore environment. This modified kinetic scheme is the simplest model consistent with the time-resolved fluorescence data for GFPs (Striker et al., 1999; present work; see below) and the hole-burning spectroscopy data upon OPE (Creemers et al., 2000).

We note that in a recent theoretical treatment of GFP photophysics (Weber et al., 1999), a fourth state (Z/Z*) representing a zwitterionic GFP chromophore was postulated in addition to the standard A, I, and B species (Weber et al., 1999). Z* could be a "dark" nonfluorescent state for some GFPs (e.g., the WTGFP), but have a finite quantum yield in the case of the other mutants. We do not mean to imply a correspondence between Z* and I_B^*, however.

Steady-state OPE and TPE fluorescence

The green emission in all three GFPs observed upon 800 nm excitation was in general agreement with the fluorescence spectra excited by OPE at 400 nm. This fact, coupled to energy conservation considerations, indicates a simultaneous absorption of two 800 nm photons. Direct evidence for the TPE phenomenon was provided by the measured power-squared dependence of the induced fluorescence intensity on the incident 800 nm photon flux density and the zero-time anisotropies upon 800 nm excitation exceeding the OPE limit of 0.4. The independence of the fluorescence intensity and anisotropy decay kinetics on the multiplicity of photon excitation also suggests that the emission occurs from the same excited states.

The TPE fluorescence clearly saturated at higher flux densities, thereby establishing an upper limit for quantitative TPE microscopy of $\sim 1.6 \times 10^{30}$ photons cm^{-2} s^{-1}. The apparent saturation may be attributed to a variety of

nonlinear optical processes, such as stimulated emission (Kusba et al., 1994), excited-state absorption (Bradley et al., 1972), photolysis (Brand et al., 1997), and ground-state depletion (Xu et al., 1996). Nonperturbative nonlinear phenomena caused by a high instantaneous field strength become important only at intensities $\geq 10^{31}$ photons cm^{-2} s^{-1} (i.e., $\geq 10^7$ V cm^{-1}) (Xu et al., 1996; Brand et al., 1997). Stimulated emission could also be excluded, since there was no overlap of the excitation wavelength of 800 nm with the fluorescence (also see Fig. 1). Fluorescence saturates at the limit of one transition per pulse per fluorophore. For a two-photon process, saturation occurs when $\sigma_2 \rho_{peak}^2 \tau_{pulse} \approx 1$ (Xu et al., 1996). Assuming a typical value of $\sigma_2 \sim 3 \times 10^{-50}$ cm^4 s $photon^{-1}$ for GFP (Xu et al., 1996), $\tau_{pulse} = 180$ fs, and a threshold value for the saturation peak intensity of $\rho_{peak} \approx 1.6 \times 10^{30}$ photons cm^{-2} s^{-1} (Fig. 2), the above relation yields ~0.014. Since OPE at 800 nm can be neglected, this result indicates that <1.4% of molecules in the focal spot are excited per laser pulse in TPE. Therefore, ground-state depletion cannot have been the dominant contribution to the observed saturation. In contrast, an analogous estimation for the OPE case suggests that excited singlet-state absorption efficiently depopulates the excited state. Indeed, Lossau et al. (1996) recently reported excited-state absorption features of WT-GFP in the spectral range 630–950 nm, peaking at ~700 nm. To perform a quantitative analysis of the deviation of the fluorescence from the power-square law as shown in Fig. 2, a rate equation formalism has to be used, taking into account the two-photon cross-sections at 800 nm reported by Xu et al. (1996) and cross-sections not yet reported for one-photon *excited-state* absorption. In conclusion, quenching of the excited singlet state by excited-state absorption at high power levels was the most likely cause for the observed deviation from the simple power law.

The relative steady-state emission intensity at 440 nm of all three systems increased upon 800 nm TPE when compared to 400 nm OPE. This may indicate a decreased ESPT rate for A* depopulation upon 800 nm excitation or, alternatively, a change in the ratio of ground-state absorption of the protonated and deprotonated species. In the former case, the electronic excited states achieved with OPE and TPE may be different due to the different photoselection rules and may consequently have different ESPT susceptibilities. In this scenario, the two-photon allowed excited state would have a lower ESPT rate, thus favoring the radiative (fluorescent) deactivation pathway. A second approach to interpreting the enhanced blue fluorescence intensity is based on the observation that absorption of 400 or 800 nm photons results in simultaneous excitation of all ground-state species to an extent dependent on their corresponding absorption cross-sections. The enhanced blue emission intensity upon 800 nm TPE indicated an increased population of A* relative to B*, suggesting that the ratio $\sigma_2(A)/\sigma_2(B)$ at 800 nm exceeds $\sigma_1(A)/\sigma_1(B)$ for 400 nm excitation. Since steady-state absorption and fluorescence excitation spectra (not shown), obtained with high-resolution spectroscopy techniques in particular (Creemers et al., 1999; Creemers et al., 2000), provide direct evidence for the simultaneous excitation of all ground-state species, we favor the second interpretation.

Fluorescence intensity decay kinetics

WT- and S65T-GFP

In the case of WT-GFP and S65T-GFP, the observed dependence of the decay kinetics on the emission wavelength was in qualitative agreement with previously reported time-resolved measurements using conventional OPE (Lossau et al., 1996). Detection at 456 nm is sensitive to both the fluorescence peaked at ~440 nm and the blue edge of the major green emission band, whereas detection at 514 nm monitors the spectrally coincident fluorescence of I_A^* and B*. The resolution of the present experiment was insufficient to resolve the decays of these two species, resulting in an apparent monoexponential decay of ~3 ns. Striker et al. (1999) have assigned lifetimes of ~3.3 ns and ~2.8 ns, respectively, to the I* and B* excited states of WT-GFP; the weighted average of both decay times was ~3.1 ns. Due to the differences in the ground-state equilibrium, the final distribution of the excited-state population favors I_A^* for WT-GFP, but B* for S65T-GFP. Thus, assuming that the energetics of the B* → B transition compared to the I_A^* → I transition is relatively more favorable in S65T-GFP, one can account for the small red shift in the green emission of the mutant protein.

The 456 nm signal, however, contains the additional subnanosecond component due to the radiative decay from A*, resulting in a biexponential kinetics. Due to the limited time-resolution of the TCSPC detection setup compared to pump-probe techniques (Lossau et al., 1996), the ~0.2 ns component should be regarded as a mean value. The ratio of the fractional intensities of the short lifetime decay component (monitored at 456 nm) for S65T-GFP and WT-GFP, f_1^{WT}/f_1^{S65T}, was ~0.5 for OPE and ~1 for TPE, consistent with the respective ratios of steady-state emission intensities at 440 nm in Fig. 1 and supporting the assignment of the short decay component to the blue emission.

RSGFP

In contrast to the monoexponential (λ_{em} = 514 nm) or biexponential (λ_{em} = 456 nm) decays for WT- and S65T-GFP, both OPE and TPE of the RSGFP mutant led to a more complex decay process, which was independent of the emission wavelength and yielded negligible blue fluorescence. As for the S65T mutant, the specific amino acid substitutions for RSGFP (F64M, S65G, Q69L) clearly lead to a shift in the ground-state equilibrium to the more deprotonated

species at pH 8. This conclusion is supported by the absence of 400 nm spectral features in the absorption or excitation spectra and the diminished blue fluorescence at 440 nm, suggesting the suppression of the protonated ground-state species (A). The complex three-exponential decays indicate an additional excited-state species with a distinct, dominant ~1.1 ns lifetime, and the most general interpretation involves the introduction of an additional (intermediate) state accessed from the B manifold (Fig. 4). In this scenario the fast B* → I* transition, which in the case of RSGFP is energetically favored (confirmed by hole-burning experiments; Creemers et al., 2000), represents the major deactivation pathway of B*. The shorter excited-state lifetime (and lower quantum yield) arises as a consequence of the larger nonradiative rate associated with the I^*_B state compared to the I^*_A state. Accordingly, the green emission arises from I* alone, as a superposition of I^*_A and I^*_B transitions to the I ground state with similar radiative, but different, nonradiative rate constants. The contribution of the B* → B emission is negligible due to the fast depopulation of B* to I^*_B. In an alternative interpretation, according to which the dominant ~1.1 ns component would be the quenched excited-state lifetime of B*, the observed fluorescence would contain (as in the case for S65T-GFP) both the I* and B* emissions, which are almost spectrally coincident and have similar excited-state lifetimes (~3 ns) in the absence of a B* → I* transition. This expectation is not consistent with the observed, dominant ~1 ns component. This reasoning prompted us to introduce the notion of a degenerate intermediate (I*) with two substates (I^*_A, I^*_B) to explain the decay time components associated with the deprotonated intermediate species of RSGFP, one of which (I^*_B) is characterized by a specific configuration with significantly higher k_{NR} (Fig. 4). The scheme also rationalizes the fact that RSGFP exhibits a spectral peak position of the green fluorescence that is characteristic for WT-GFP, although the ground-state distribution is strongly shifted toward the red (i.e., I and B forms), as with S65T-GFP. In both WT-GFP and RSGFP the green fluorescence arises predominantly from the radiative I* → I transition.

A plausible origin for the fivefold difference in the nonradiative rates associated with the two I* substates may lie in the details of the hydrogen-bonding and hydration networks that are affected by the specific mutations in RSGFP. We anticipate that further insight will be provided by a high-resolution crystal structure for this mutant. A survey of the known crystal structures of GFP mutants reveals that the so-called yellow fluorescence protein (YFP) mutants of GFP also have the S65G mutation (Wachter et al., 1998). While the chromophore in YFP is more rigid due to the stacking interaction with the phenol ring from the T203Y substitution (Wachter et al., 1998), cavity-creating mutations (such as the S65G exchange) generally lead to increased flexibility of the protein microenvironment (Eriksson et al., 1992). In addition, Gln-69 is involved in the hydrogen-bonding network surrounding the chromophore (Brejc et al., 1997; Wachter et al., 1998), and in YFP is specifically implicated in an interaction with the carbonyl oxygen of the chromophore imidazolinone ring (Wachter et al., 1998). The Q69L mutation will almost certainly disrupt some of these bonds and affect the photophysics of the chromophore. The cumulative effect of the mutations in RSGFP is most likely an increased flexibility of the chromophore, which may account for the faster fluorescence depolarization associated with the proposed B* → I^*_B → I pathway.

Similar multiexponential fluorescence ("dispersive kinetics") in the range of 450–600 nm were reported by Lossau et al. for a blue-shifted mutant (BFP11) excited at 350 nm and having a mean decay time of 0.9 ns (Lossau et al., 1996). This fluorescence was thought to originate from a single excited-state species based on the observation of only one ground-state species, attributed in BFP11 to the protonated form of the chromophore. For RSGFP a similar situation prevails, but the deprotonated ground-state species predominates. Thus, an analogous interpretation could attribute the dispersive decay kinetics of RSGFP to dielectric relaxation phenomena of the chromophore in its protein environment. Supporting evidence comes from low-temperature Stark spectra of WT-GFP (Chattoraj et al., 1996) and S65T-GFP (Bublitz et al., 1998), indicating large dipole moment changes between ground and excited states, and from the anisotropy data discussed below.

Fluorescence anisotropy decay kinetics

In all cases the initial anisotropy values measured with 800 and 400 nm excitation approached the theoretical limits of 0.57 and 0.40 for TPE and OPE, respectively. The measured OPE r_0 agreed well with the value of ~0.39 for humanized red-shifted GFP recently reported by Partikian et al. (1998). In conclusion, the one- and two-photon induced fluorescence anisotropies of the GFPs studied were found to obey the theory derived for polyene-like molecules (Eq. 2), according to which the 400 nm absorption dipole or correspondingly the dominant element of the 800 nm two-photon transition tensor is almost colinear with the 514 nm emission transition dipole ($\beta \approx 0$).

There was good agreement within experimental uncertainty between the rotational relaxation times in OPE and TPE, as expected since rotational rates are determined only by the size and shape of the probe molecule and the nature of its microenvironment. The finding also confirms the absence of significant heating by the intense laser beam in TPE. Such an effect would have caused a decrease of both the fluorescence intensity and rotational decay times. A mean rotational correlation time calculated from the data for all the GFPs studied was ~16 ns. Due to the absence of any measured fast (subnanosecond) anisotropy decay, this value corresponds to the rotation of the entire protein without

significant contributions from segmental motions of the chromophore. The rotational correlation times obtained for S65T-GFP were comparable to the ~19 ns previously reported for this mutant in PBS (pH 7.4) using OPE at 492 nm (Swaminathan et al., 1997).

The theoretical value for the rotational correlation time of GFP, assuming the rotation of a 31-kDa isotropic rotator (Ormo et al., 1996) and a hydrated volume of a typical protein of $\sim 1\ cm^3\ g^{-1}$ (Cantor and Schimmel, 1980), would be $\phi_{sp} \sim 13$ ns. Since the x-ray structure of GFP is known, one can readily compare the experimental value of ϕ with the theoretical predictions in more detail. The plane of the chromophore group lies buried inside the cylinder-shaped protein oriented at an angle of ~60° to the symmetry axis of the cylinder of 2.4 nm diameter and 4.2 nm height (Ormo et al., 1996; Yang et al., 1996). Three anisotropy decay components are predicted theoretically using a prolate ellipsoid model with an axial ratio of 1.75 (Kawski, 1993), yielding correlation time components expressed as a function of the calculated isotropic correlation time ϕ_{sp} of $\phi_1 = 1.34 \times \phi_{sp}$, $\phi_2 = 1.22 \times \phi_{sp}$, $\phi_3 = 0.95 \times \phi_{sp}$, with fractional intensities of 2%, 62%, and 36%, respectively. In the experimental anisotropy decays of WT- and S65T-GFP, however, only a single rotational correlation time could be resolved, corresponding to the average of the three theoretically derived correlation time components weighted by their fractional intensities. The theoretical average is 14.5 ns, in good agreement with the experimental values (Table 2). These values assume that the protein is in monomeric form, which is expected for the concentrations of proteins used in these experiments (Ward, 1998).

In contrast to the monoexponential anisotropy decay of WT- and S65T-GFP, the red-shifted mutant RSGFP exhibited a behavior indicative of an apparent internal (local) motion of the chromophore, due to increased flexibility and/or passage between the different excited-state species. This interesting finding is under further investigation. The global rotational correlation time, however, was in agreement with that of WT- and S65T-GFP, reflecting the rotational motion of the entire protein and consistent with the expectation that these mutations do not substantially alter the tertiary structure of the protein. Such an internal motion has been recently invoked in the context of shortened excited-state lifetimes and fast ground-state recovery in specific red-shifted GFP mutants (Kummer et al., 1998).

CONCLUSION

Time-resolved detection of multiphoton-induced anisotropic fluorescence using TCSPC techniques confirms that a higher degree of molecular orientation for TPE is obtained in comparison to OPE. TPE thus offers a more sensitive measurement of fluorescence anisotropy decays of GFPs when probing the dynamics and structure of nanometer-scale biological systems using its higher intrinsic anisotropy. In particular, this potential could be exploited in in vivo fluorescence microspectroscopy and diffusion studies using GFP or GFP-tagged molecules. Despite the complexity of the fluorescence intensity and anisotropy decay kinetics of RSGFP, its significantly shorter average lifetime (~1.7 ns) would allow its discrimination in fluorescence lifetime imaging microscopy from other spectrally similar GFPs (e.g., S65T-GFP) exhibiting the usual ~3 ns fluorescence lifetime.

We thank Gudrun Heim for expert technical assistance and George Striker for a critical reading of the manuscript. The experimental work was carried out in the Femtosecond Research Center at the University of Strathclyde.

V.S. was supported by a long-term fellowship from the Human Frontiers Science Program Organization. A.V. acknowledges support from British Nuclear Fuels plc.

REFERENCES

Bastiaens, P. I. H., and T. M. Jovin. 1996. Microspectroscopic imaging tracks the intracellular processing of a signal transduction protein: fluorescent-labeled protein kinase C βI. *Proc. Natl. Acad. Sci. USA.* 93: 8407–8412.

Bennett, B. D., T. L. Jetton, G. Ying, M. A. Magnuson, and D. W. Piston. 1996. Quantitative subcellular imaging of glucose metabolism within intact pancreatic islets. *J. Biol. Chem.* 271:3647–3651.

Bewersdorf, J., R. Pick, and S. W. Hell. 1998. Multifocal multiphoton microscopy. *Opt. Lett.* 23:655–657.

Bradley, D. J., M. H. R. Hutchinson, H. Koetser, T. Morrow, G. H. C. New, and M. S. Petty. 1972. Interactions of picosecond laser pulses with organic molecules. I. Two-photon fluorescence quenching and singlet states excitation in rhodamine dyes. *Proc. R. Soc. Lond. A.* 328:97–121.

Brand, L., C. Eggeling, C. Zander, K. H. Drexhage, and C. A. M. Seidel. 1997. Single-molecule identification of coumarin-120 by time-resolved fluorescence detection: comparison of one- and two-photon excitation in solution. *J. Phys. Chem. A.* 101:4313–4321.

Brejc, K., T. K. Sixma, P. A. Kitts, S. R. Kain, R. Y. Tsien, M. Ormo, and S. J. Remington. 1997. Structural basis for dual excitation and photoisomerization of the Aequorea victoria green fluorescent protein. *Proc. Natl. Acad. Sci. USA.* 94:2306–2311.

Bublitz, G., B. A. King, and S. G. Boxer. 1998. Electronic structure of the chromophore in green fluorescent protein (GFP). *J. Am. Chem. Soc.* 120:9370–9371.

Callis, P. R. 1993. On the theory of two-photon induced fluorescence anisotropy with application to indoles. *J. Chem. Phys.* 99:27–37.

Cantor, C. R., and P. R. Schimmel. 1980. Biophysical Chemistry II. W. H. Freeman and Company, San Francisco.

Chattoraj, M., B. A. King, G. U. Bublitz, and S. G. Boxer. 1996. Ultra-fast excited state dynamics in green fluorescent protein: multiple states and proton transfer. *Proc. Natl. Acad. Sci. USA.* 93:8362–8367.

Chen, S. Y., and B. W. VanDerMeer. 1993. Theory of two-photon induced fluorescence anisotropy decay in membranes. *Biophys. J.* 64:1567–1575.

Creemers, T. M. H., A. J. Lock, V. Subramaniam, T. Jovin, and S. Völker. 1999. Three photoconvertible forms of Green Fluorescent Protein identified by spectral hole-burning. *Nat. Struct. Biol.* 6:557–560.

Creemers, T. M. H., A. J. Lock, V. Subramaniam, T. M. Jovin, and S. Völker. 2000. Photophysics and optical switching in green fluorescent protein mutants. Proc. Natl. Acad. Sci. USA. In press.

Delagrave, S., R. E. Hawtin, C. M. Silva, M. M. Yang, and D. C. Youvan. 1995. Red-shifted excitation mutants of the green fluorescent protein. *BioTechnology.* 13:151–154.

Denk, W., D. W. Piston, and W. W. Webb. 1995. Two-photon molecular excitation in laser-scanning microscopy. *In* Handbook of Biological

Confocal Microscopy. J. P. Pawley, editor. Plenum Press, New York. 445–458.

Denk, W., J. H. Strickler, and W. W. Webb. 1990. Two-photon laser scanning fluorescence microscopy. *Science.* 248:73–76.

Eriksson, A. E., W. A. Baase, X.-J. Zhang, D. W. Heinz, M. Blaber, E. P. Baldwin, and B. W. Matthews. 1992. Response of a protein structure to cavity-creating mutations and its relation to the hydrophobic effect. *Science.* 255:178–183.

Gryczynski, I., H. Malak, and J. R. Lakowicz. 1995. Three-photon induced fluorescence of 2,5-diphenyloxazole with a femtosecond Ti:sapphire laser. *Chem. Phys. Lett.* 245:30–35.

Haupts, U., S. Maiti, P. Schwille, and W. W. Webb. 1998. Dynamics of fluorescence fluctuations in green fluorescent protein observed by fluorescence correlation spectroscopy. *Proc. Natl. Acad. Sci. USA.* 95: 13573–13578.

Jovin, T. M., M. Bartholdi, W. L. Vaz, and R. H. Austin. 1982. Rotational diffusion of biological macromolecules by time-resolved delayed luminescence (phosphorescence, fluorescence) anisotropy. *Ann. N.Y. Acad. Sci.* 366:176–196.

Kawski, A. 1993. Fluorescence anisotropy: theory and applications of rotational depolarization. *Crit. Rev. Anal. Chem.* 23:459–529.

Kohler, R. H., J. Cao, W. R. Zipfel, W. W. Webb, and M. R. Hanson. 1997. Exchange of protein molecules through connections between higher plant plastids. *Science.* 276:2039–2042.

Kummer, A. D., C. Kompa, H. Lossau, F. Pöllinger-Dammer, M. E. Michel-Beyerle, C. M. Silva, E. J. Bylina, W. J. Coleman, M. M. Yang, and D. C. Youvan. 1998. Dramatic reduction in fluorescence quantum yield in mutants of Green Fluorescent Protein due to fast internal conversion. *Chem. Phys.* 237:183–193.

Kusba, J., V. Bogdanov, I. Gryczynski, and J. R. Lakowicz. 1994. Theory of light quenching: effects on fluorescence polarization, intensity, and anisotropy decays. *Biophys. J.* 67:2024–2040.

Lakowicz, J. R., I. Gryczinski, and E. Danielsen. 1992. Anomalous differential polarized phase angles for two-photon excitation with isotropic depolarizing rotations. *Chem. Phys. Lett.* 191:47–53.

Lossau, H., A. Kummer, R. Heinecke, F. Pöllinger-Dammer, C. Kompa, G. Bieser, T. Jonsson, C. M. Silva, M. M. Yang, D. C. Youvan, and M. E. Michel-Beyerle. 1996. Time-resolved spectroscopy of wild-type and mutant Green Fluorescent Proteins reveals excited state deprotonation consistent with fluorophore-protein interactions. *Chem. Phys.* 213:1–16.

Mahajan, N. P., K. Linder, G. Berry, G. W. Gordon, R. Heim, and B. Herman. 1998. Bcl-2 and Bax interactions in mitochondria probed with green fluorescent protein and fluorescence resonance energy transfer. *Nature Biotech.* 16:547–552.

Malak, H., F. N. Castellano, I. Gryczynski, and J. R. Lakowicz. 1997. Two-photon excitation of ethidium bromide labeled DNA. *Biophys. Chem.* 67:35–41.

Misteli, T., and D. L. Spector. 1997. Applications of the green fluorescent protein in cell biology and biotechnology. *Nature Biotech.* 15:961–964.

Miyawaki, A., J. Llopis, R. Heim, J. M. McCaffery, J. A. Adams, M. Ikura, and R. Y. Tsien. 1997. Fluorescent indicators for Ca^{2+} based on Green Fluorescent Proteins and calmodulin. *Nature.* 388:882–887.

Nageswara Rao, B. D., M. D. Kemple, and F. G. Prendergast. 1980. Proton nuclear magnetic resonance and fluorescence spectroscopic studies of segmental mobility in aequorin and a green fluorescent protein from *Aequoria forskalea. Biophys. J.* 32:630–632.

Ng, T., A. Squire, G. Hansra, F. Bornancin, C. Prevostel, A. Hanby, W. Harris, D. Barnes, S. Schmidt, H. Mellor, P. I. H. Bastiaens, and P. J. Parker. 1999. Imaging protein kinase C alpha activation in cells. *Science.* 283:2085–2089.

Niswender, K. D., S. M. Blackman, L. Rohde, M. A. Magnuson, and D. W. Piston. 1995. Quantitative imaging of green fluorescent protein in cultured cells: comparison of microscopic techniques, use in fusion proteins and detection limits. *J. Microsc.* 180:109–116.

Ormo, M., A. B. Cubitt, K. Kallio, L. A. Gross, R. Y. Tsien, and S. J. Remington. 1996. Crystal structure of the *Aequorea victoria* green fluorescent protein. *Science.* 273:1392–1395.

Palm, G. J., A. Zdanov, G. A. Gaitanaris, R. Stauber, G. N. Pavlakis, and A. Wlodawer. 1997. The structural basis for spectral variations in green fluorescent protein. *Nat. Struct. Biol.* 4:361–365.

Partikian, A., B. Ölveczky, R. Swaminathan, Y. Li, and A. S. Verkman. 1998. Rapid diffusion of green fluorescent protein in the mitochondrial matrix. *J. Cell Biol.* 140:821–829.

Patterson, G. H., S. M. Knobel, W. D. Sharif, S. R. Kain, and D. W. Piston. 1997. Use of the green fluorescent protein and its mutants in quantitative fluorescence microscopy. *Biophys. J.* 73:2782–2790.

Perozzo, M. A., K. B. Ward, R. B. Thompson, and W. W. Ward. 1988. X-ray diffraction and time-resolved fluorescence analyses of Aequorea green fluorescent protein crystals. *J. Biol. Chem.* 263:7713–7716.

Presley, J. F., N. B. Cole, T. A. Schroer, K. Hirschberg, K. J. M. Zaal, and J. Lippincott-Schwartz. 1997. ER-to-Golgi transport visualized in living cells. *Nature.* 389:81–85.

Striker, G., V. Subramaniam, C. A. M. Seidel, and A. Volkmer. 1999. Photochromicity and fluorescence lifetimes of Green Fluorescent Protein. *J. Phys. Chem. B.* 103:8612–8617.

Svoboda, K., W. Denk, D. Kleinfeld, and D. W. Tank. 1997. In vivo dendritic calcium dynamics in neocortical pyramidal neurons. *Nature.* 385:161–165.

Swaminathan, R., C. P. Hoang, and A. S. Verkman. 1997. Photobleaching recovery and anisotropy decay of Green Fluorescent Protein GFP-S65T in solution and cells: cytoplasmatic viscosity probed by Green Fluorescent Protein translational and rotational diffusion. *Biophys. J.* 72: 1900–1907.

Tsien, R. Y. 1998. The green fluorescent protein. *Annu. Rev. Biochem.* 67:509–544.

Volkmer, A., D. A. Hatrick, and D. J. S. Birch. 1997. Time-resolved nonlinear fluorescence spectroscopy using femtosecond multiphoton excitation and single-photon timing detection. *Meas. Sci. Technol.* 8:1339–1349.

Wachter, R. M., M. A. Elsliger, K. Kallio, G. T. Hanson, and S. J. Remington. 1998. Structural basis of spectral shifts in the yellow-emission variants of green fluorescent protein. *Structure.* 6:1267–1277.

Wan, C. Z., and C. K. Johnson. 1994. Time-resolved anisotropic two-photon spectroscopy. *Chem. Phys.* 179:513–531.

Ward, W. 1998. Biochemical and physical properties of green fluorescent protein. *In* Green Fluorescent Protein: Properties, Applications and Protocols. M. Chalfie and S. Kain, editors. Wiley-Liss, New York. 45–75.

Weber, W., V. Helms, J. A. McCammon, and P. W. Langhoff. 1999. Shedding light on the dark and weakly fluorescing states of green fluorescent proteins. *Proc. Natl. Acad. Sci. USA.* 96:6177–6182.

Xu, C., and W. W. Webb. 1996. Measurement of two-photon excitation cross sections of molecular fluorophores with data from 690 to 1050 nm. *J. Opt. Soc. Am. B.* 13:481–491.

Xu, C., W. Zipfel, J. B. Shear, R. M. Williams, and W. W. Webb. 1996. Multiphoton fluorescence excitation: new spectral windows for biological nonlinear microscopy. *Proc. Natl. Acad. Sci. USA.* 93:10763–10768.

Yang, F., L. G. Moss, and G. N. Phillips. 1996. The molecular structure of Green Fluorescent Protein. *Nature Biotech.* 14:1246–1251.